Microstructural analysis of the type-II boundary region in Alloy 152 weld

Seung Chang Yoo, Kyoung Joon Choi and Ji Hyun Kim*
School of Mechanical and Nuclear Engineering,
Ulsan National Institute of Science and Technology, Ulsan, Republic of Korea
**Corresponding author: kimjh@unist.ac.kr*

1. Introduction

One important issue deciding the life of nuclear power plants is the susceptibility of structural materials to stress corrosion cracking (SCC). SCC is caused by two key factors: 1) stress from high pressure and radiation, and 2) corrosion from the corrosive environment of nuclear power plants. Dissimilar metal weld (DMW) joints are known to be susceptible to SCC because of 1) residual stress induced by the difference of the thermal conductivity and thermal expansion coefficients between the base metal and weld metal, 2) the residual stress caused by the welding process and oxidation, and 3) the complicated microstructure at the weld fusion boundary because of repeated welding heat and compositional gradients [1].

Alloy 152 is frequently used as a filler metal for joining austenitic Ni-based Alloy 690 and low-alloy steel (LAS) A533 Gr. B. This DMW joint is commonly used in nuclear power plants in pressure vessel nozzles or steam generator nozzles. Before DMW joints were performed with Alloy 152 filler metal, Alloy 182 was used as a filler material. However, Alloy 182 is found to be particularly susceptible to SCC after long-term operation in power plants. For this reason, the filler metal was replaced with Alloy 152. To date, there is no experience of SCC in the weld side of DMW joints where Alloy 152 is used as a filler metal in operation power plants. However, it is believed that the current operational experience is not sufficient to conclude that high Cr, Ni alloys are immune to SCC.

Many studies emphasize the importance of the SCC of the weld fusion boundary because of the complex microstructure near the fusion boundary and because of the residual stress induced by oxidation or the welding process. Seifert et al. [2] conducted an investigation on SCC growth behavior in the transition region of an Alloy 182-SA 508 Cl.2 weld joint heat treated under simulated boiling water reactor normal water chemistry (BWR/NWC) conditions. They conclude that the weld metals are more susceptible to SCC growth and that most cracks are blunted by the fusion boundary. However, they also found that some cracking occurs along the fusion boundary, often in an area with high hardness.

Nelson et al. [3] investigated a DMW of Monel 409 stainless steel and American Iron and Steel Institute (AISI) 1080 alloy and found a type-II boundary, which exists parallel to the fusion boundary in the dilution zone. They conclude that the type-II boundary is a potential path for crack growth. While there are several theories for the mechanisms of the type-II boundary formation, they conclude that the type-II boundary forms from the allotropic δ-γ transformation at the base metal in the elevated austenitic temperature range. Moreover, many other crack growth experiments conclude that the type-II boundary and fusion boundary region of the weld metal are susceptible to SCC [4]. Hou et al. [4, 5] investigate the microstructure and mechanical properties of the DMW of Alloy 182 and low-alloy steel A533 Gr. B. Using the tensile test, they found that type-II boundaries are high angle grain boundaries, which are more susceptible to SCC than low-angle grain boundaries.

As the operation time of nuclear power plants using DMWs of Alloy 152 and A533 Gr. B increases, these DMWs must be evaluated for their resistance to SCC for long-term operations. However, only few studies have investigated the thermal aging effects induced by long-term operations at high temperature.

Type-II boundary is known as a potential crack path from the results of crack growth test at DMW without any heat treatment. So the analysis about type-II boundary with applying heat treatment could be helpful to evaluate the susceptibility to SCC of structural materials.

The objective of this study is to analyze the detailed microstructure of the type-II boundary region in the DMW of Alloy 152 and A533 Gr. B, after applying heat treatment simulating thermal aging effect of a nuclear power plant operation condition to evaluate the susceptibility of this region to SCC. The microstructure of the type-II boundary region in the DMW of Alloy 152 and A533 Gr. B were analyzed with an energy dispersive x-ray spectroscope attached to a scanning electron microscope (SEM-EDS), electron backscatter diffraction (EBSD), and a nanoindentation test.

Table 1. Composition of each alloy of DMW

Material	C	Al	Si	P	S	Cr	Mn	Fe	Co	Ni	Cu	Nb+Ta	Mo	Ti
Alloy 690	0.03		0.07		<0.001	29.50	0.20	9.90		59.50	0.01			
Alloy 152	0.04	0.24	0.46	<0.003	<0.001	29.04	3.56	9.36	<0.01	55.25	<0.01	1.84	0.01	0.15
A533 Gr.B	0.22		0.19	0.01	0.012	0.18	1.28	97.12		0.51			0.48	

2. Experiment

2.1 Materials

DMW samples were fabricated by Argonne National Laboratory. Alloy 690 and low-alloy steel A533 Gr. B were joined with austenitic Alloy 152 filler metal by multi-pass shielded metal arc welding. The composition of each material is shown in Table 1. The welding process was qualified by the American Society of Mechanical Engineers (ASME) section IX [6]. After the buttering procedure with low-alloy steel and Alloy 152, the samples were post-weld heat treated at 607℃–635℃ for 3 h. The experimental specimens were cut from the mock-up samples by wire-cutting from the weld root area, which contained the fusion boundary between Alloy 152 and low-alloy steel A533 Gr. B. Table 2 shows the specimen ID, simulated operation time and simulation aging time and temperature of each specimen. The analysis area is limited to the weld root area of the whole specimen to minimize the difference of heat affect caused by the welding process.

2.2 Heat treatment conditions

The heat treatment was conducted to simulate thermal aging at LWR environment by long term operation at 320˚C. The accelerated temperature for thermal aging simulation is decided to 450˚C which is the highest temperature not making any excessive carbides or sigma phase which would not be created after long term operated at 320˚C. Equation (1) is used for calculating aging time needed to simulation.

$$\frac{t_{aging}}{t_{ref}} = exp\left[-\frac{Q\left(\frac{1}{T_{ref}}-\frac{1}{T_{aging}}\right)}{R}\right] \quad (1)$$

Here, t_{aging} is the heat treatment time needed to simulate thermal aging at a nuclear power plant, and t_{ref} is the time being simulated. The heat treatment temperature is T_{aging} (450℃), and T_{ref} is the actual operation temperature of the nuclear power plant (320℃). The activation energy for Cr diffusion is Q, which is 125 kJ/mol [8], and R is the gas constant. Because Cr plays an essential role in the precipitation and corrosion resistance, which influences the SCC resistance, the activation energy is selected for Cr diffusion. We produce four specimen types with which we simulated the simulation aging time of 15 years, 30 years, 60 years, and non-thermally aged. The corresponding simulation times are 1375, 2750, and 5500 h heat treated at 450℃, and non-heat treated, respectively. Fig. 1 shows the graph of estimated heat treatment time required for simulating the operation time at 320℃.

Table 2. Specimen ID, simulated operation time, and simulation aging time of each specimen

Specimen ID	Simulated operation time	Simulation aging and temperature
As-welded	As welded	As welded
HT450_Y15	15 years	1373 hours at 450℃
HT450_Y30	30 years	2750 hours at 450℃
HT450_Y60	60 years	5500 hours at 450℃

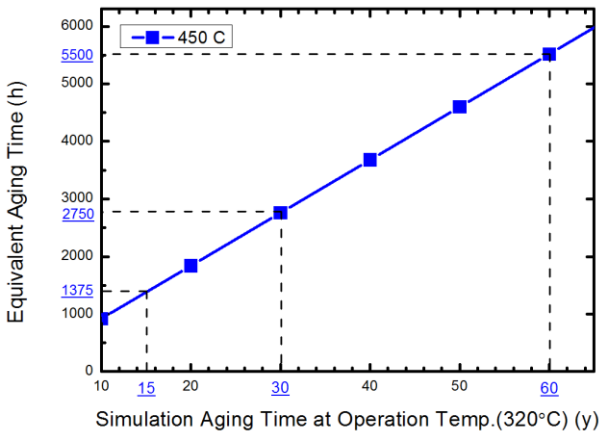

Fig. 1. Equivalent aging time required for simulating simulation aging time at 320℃

2.3 Preparation for experiments and experimental conditions

Every specimen used for experiments was cut off from weld root of fusion boundary region of each heat treated mock-up samples. The specimens are polished with sand papers, diamond paste and colloidal silica up to 0.05 μm, and polished about 1 h with 0.05-μm silica to remove mechanical deformations caused by polishing. The samples were then final polished with a vibratory polisher. Finally, the specimens were etched with 20% HNO3 + HCl solution for about 3 minutes.

The microstructure characterizations were conducted in the FEI Nanonova 230 Field Emission Scanning Electron Microscope with an attached EDS and EBSD. For the SEM-EDS analysis, an acceleration voltage of 10 kV and a current of 0.64 nA were used. For EBSD, an acceleration voltage of 30 kV, a current of 0.83 nA, a tilt angle of 70°, and a step size of 0.3 μm were used. The scanned area for the EBSD analysis was about 60 μm x 175 μm.

Nanoindentation tests were performed in the Agilent Technologies Nano Indenter G200. The continuous stiffness measurement (CSM) technique of the Nano Indenter XP with a three-sided pyramidal Berkovich tip was used for the whole nanoindentation test. The experimental conditions used for nanoindentation were a total penetration depth of 2000 nm, a strain rate of 0.05 s^{-1}, and a Poisson's ratio of 0.3.

3. Results

3.1 Microstructure analysis with scanning electron microscopy

As shown in Fig. 2, type-II boundaries were found in the whole specimen. The type-II boundaries seem to be arranged and be shifted away from the fusion boundary as the heat treatment was conducted.

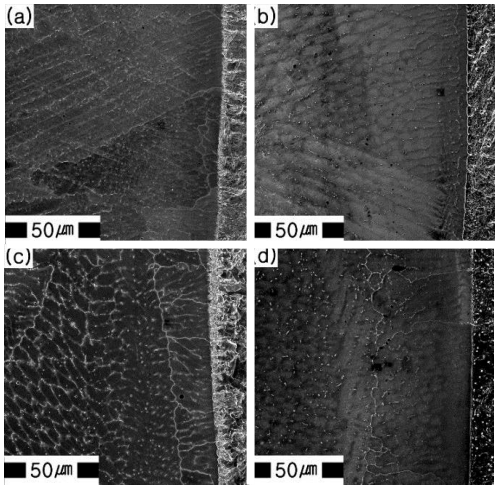

Fig. 2. Microstructures near type-II boundaries of (a) as-welded, (b) HT450_Y15, (c) HT450_Y30, and (d) HT450_Y60

According to Nelson et al. [3], the fusion boundary becomes a γ-FCC grain boundary between Fe austenite base metal and Ni-rich FCC weld metal from δ-γ transformations of the base metal during welding. Then, the γ-FCC grain boundary diffuses into the weld metal at the austenite temperature range. The austenite temperature range could vary because of the composition gradient across the fusion boundary and type-II boundary into the weld metal. The SEM images are compatible with this thesis, as the type-II boundaries seems to be shifted away from fusion boundary as the heat treatment was conducted. Over the type-II boundaries, a dendrite structure, which is a typical structure in weld metals formed by heat diffusion during the welding process, was found.

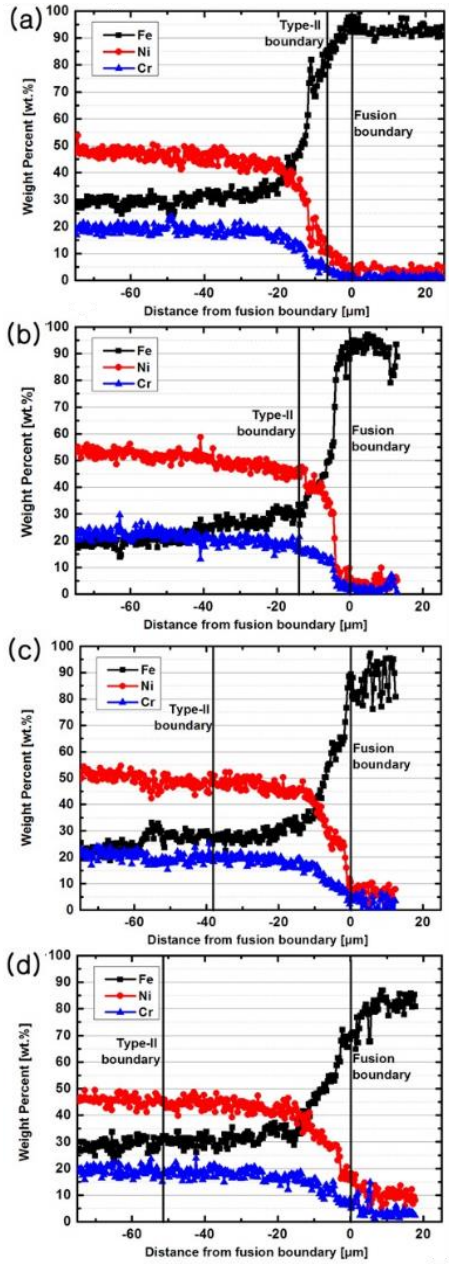

Fig. 3. EDS analysis data of (a) as-welded, (b) HT450_Y15, (c) HT450_Y30 and (d) HT450_Y60

From the chemical composition analysis with the EDS, no composition trends were detected by the existence of type-II boundary as shown in Fig. 3. However, at the narrow zone between the type-II boundary and fusion boundary, the change of composition was sharp. Furthermore, slight increasing of chromium contents were observed at the narrow zone between the fusion boundary and type-II boundary as the heat treatment progressed. This is coincidence results with previous studies, which concluded that the chromium dilution zone at the weld metal decreased as the heat treatment progressed [7].

3.2 Orientation analysis with orientation imaging microscopy

Orientation imaging microscopy with EBSD was performed near the type-II boundary and fusion boundary. The misorientation of grain boundaries and the grain average misorientation (GAM) were analyzed for each specimen. For better data accuracy, software clean-up processes were applied by the process including the grain confidence index standardization and the grain dilation for GAM analysis. However, it was not applied to the misorientation analysis because the misorientation analysis could be dramatically changed by the clean-up process because very small misorientation is often observed that could be ignored or modified by the clean-up process.

The grain boundary characters play an important role in the resistance to SCC growth or initiation. Previous studies often categorize the grain boundaries into three groups: low-angle grain boundaries, coincidence site lattice (with Σ numbers), and high-angle grain boundaries. Generally, low-angle grain boundaries and low-number-Σ boundaries are known to have resistance to SCC [9]. High-angle grain boundaries have high energy that could induce the segregation and formation of precipitates. Because most precipitates formed in nickel-based weld metals are chromium precipitates, the chromium dilution zone could be formed near high-angle grain boundaries, which could increase the susceptibility of alloys to SCC [3-5].

GAM is a local misorientation parameter defined by the average misorientation within neighboring grains. It is noted that previous studies about cold worked metals conclude that GAM is proportional to the local strain [4, 10]. Therefore, residual strain induced by welding or oxidation could be analyzed with the GAM value of the EBSD analysis. The residual strain plays a key role in the susceptibility of alloys to SCC [4, 5].

As shown in Fig. 4, a slight increase of low-angle grain boundaries was observed as the heat treatment progressed. The GAM was highest at the narrow zone between the type-II boundary and fusion boundary as shown in Fig. 5, and no significant changes occurred by heat treatment. Several studies noted that GAM is proportional to the residual strain, which could increase the susceptibility of alloys to SCC [4, 5].

Therefore, the narrow zone between the type-II boundary and the fusion boundary could be more susceptible to SCC than any other region.

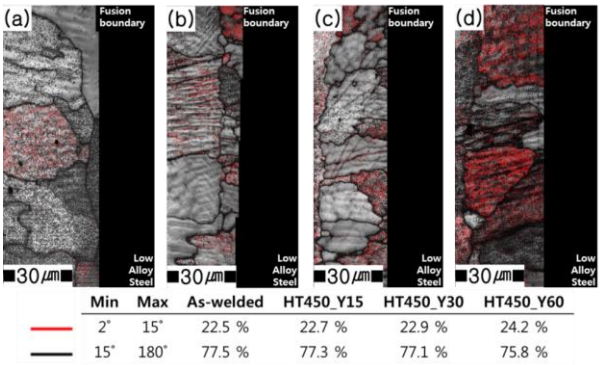

Fig. 4. Map of grain boundary misorientation angle: (a) as-welded, (b) HT450_Y15, (c) HT450_Y30, and (d) HT450_Y60

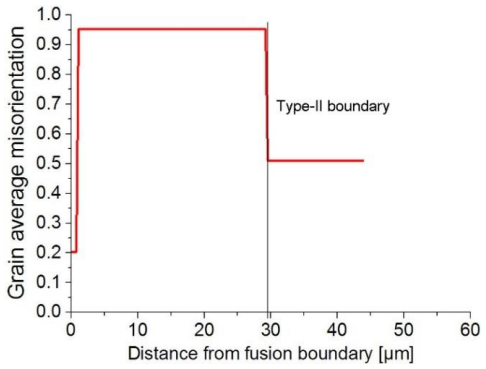

Fig. 5. GAM analysis result at arbitrary line intersecting fusion boundary and type-II boundary of HT450_Y60

3.3 Nanoindentation

Nanoindentations were performed in the specimen 1) within the narrow zone between the type-II boundary and fusion boundary, as shown in region (a) of Fig. 6 or 2) within the region about 80 μm away from the fusion boundary in the weld metal, as shown in region (b) of Fig. 6. In both tests, the nanohardness was lowest for the non-heat-treated specimen as shown in Fig. 7. The hardness increased for the heat-treated specimen simulating 15 years, and the hardness decreased for heat-treated specimen simulating more than 15 years of service. The influence of the heat treatment was less effective in the region away from the fusion boundary. The hardness was slightly changed by the heat treatment, but this change was much smaller than the change near the type-II boundary.

The average hardness was higher in the narrow zone between the type-II boundary and fusion boundary. This result is compatible with the result from previous studies, concluding that residual strain at the narrow

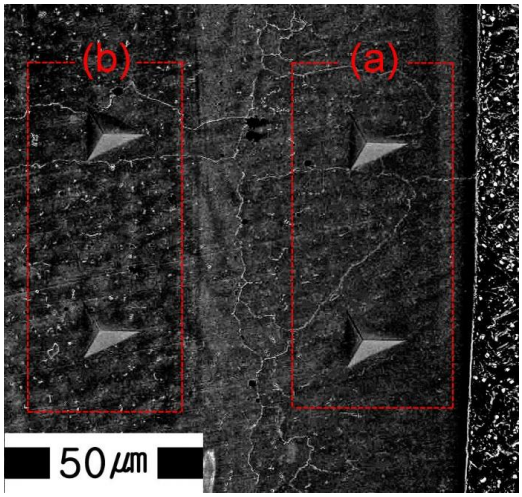

Fig. 6. Nanoindentation tracks

zone between the type-II boundary and fusion boundary was the highest [4, 5].

There are several factors affecting the hardness in the weld region: precipitates, residual strain and grain boundary misorientations near grain boundaries, and so on. Therefore, the major factors for the change of the hardness during the heat treatment might be different with treatment time.

4. Discussions

4.1 The effect of thermal aging

The purpose of this study is to analyze the detailed microstructure near the type-II boundary in the weld metal side of the DMW between Alloy 152 and A533 Gr. B with heat treatment to simulate thermal aging.

From scanning electron microscopy analysis, the type-II boundaries were found in the all specimen including as-welded and aged samples. Moreover, the type-II boundaries seem to be aligned and then be shifted away from the fusion boundary as the heat treatment proceeded. From previous studies, crack growth through the type-II boundary was observed; however, the concept of the type-II boundary was established recently, so few studies explicitly discuss the type-II boundary. From the images of the cracks, it is clear that cracking occurs along the type-II boundary [4, 5, 11]. As a result, the migration of the type-II boundary could induce several SCC related problems. Further experiments, including a crack growth test, will be needed to confirm this.

After heat treatment, the EDX result shows increasing chromium content in the dilution zone of weld metal. The chromium dilution zone is formed by the precipitation of carbides with the carbon from the base metal near the fusion boundary. From this result,

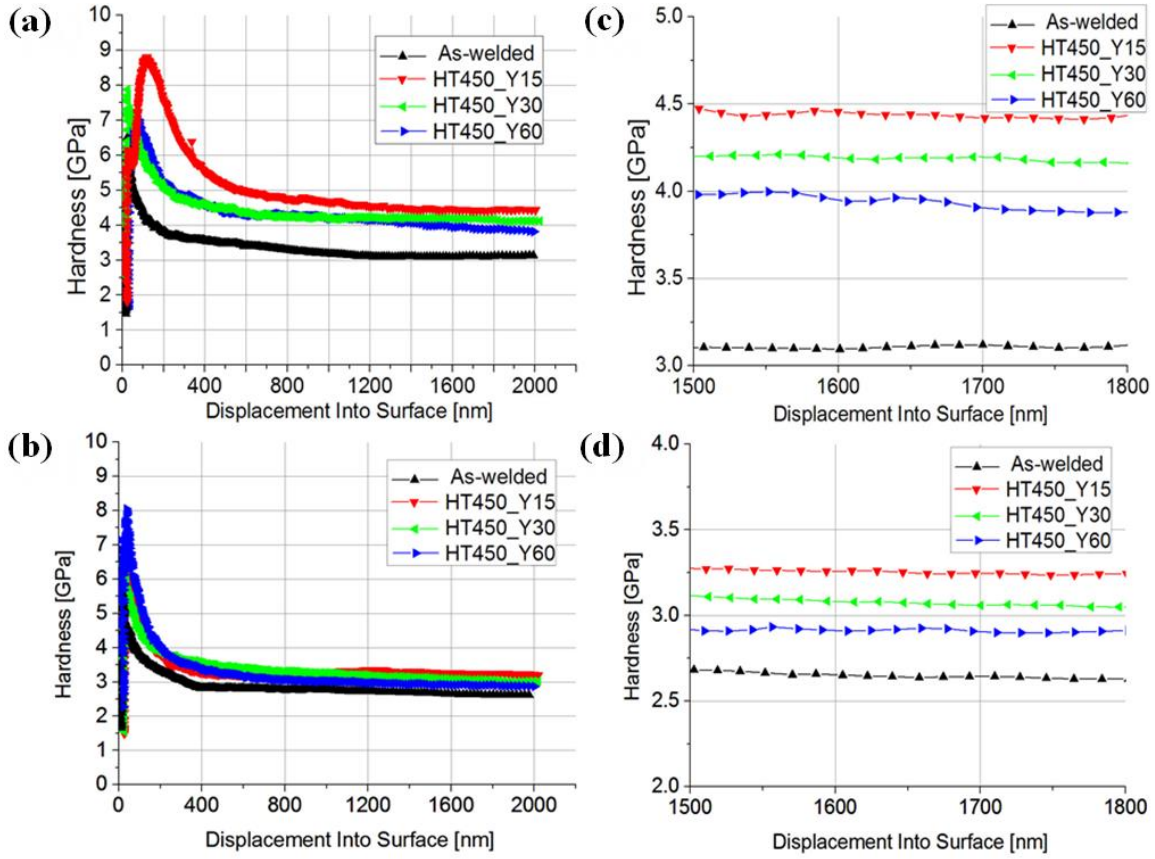

Fig. 7. Hardness-displacement into surface graphs of nanoindentation tests. (a) and (c) are result tested in the narrow zone between type-II boundary and fusion boundary, (b) and (d) are result tested over the type-II boundary. (c) and (d) are a more magnified view of (a) and (b), respectively

the precipitates could be formed in the early stages of thermal aging and coarsen or migrate during later stages of thermal aging. Previous studies found that the precipitates were formed at the early stage of thermal aging, and they only coarsen or migrate to the highly energetic boundary [12]. The coarsening of precipitates is known to reduce the resistivity of alloys to SCC.

From the EBSD analysis, an increase in the low-angle grain boundaries is observed with the heat treatment. Generally, low-angle grain boundaries are known to reduce susceptibility to SCC [7]. Furthermore, a high GAM value is observed at the narrow zone between the type-II boundary and fusion boundary. Previous studies conclude that GAM value is proportional to residual strain which could increase susceptibility of materials to SCC [4, 10].

4.2 Nanohardness based analysis

As seen from the nanoindentation test results, the nanohardness was highest for the heat treatment simulating an operation time of 15 years and was lowest for the non-heat-treated specimen. Based on thermal aging effects described above, the parameters affecting nanohardness should be considered during the heat treatment process. There were several studies conclude that precipitations were formed at early stage of heat treatment, which is coincidence result with this result.

At the early stage of heat treatment, i.e., until heat treatment simulating an operation time of 15 years, the precipitation of chromium carbide might significantly affect the nanohardness. For this reason, the hardness of the specimen simulating an operation time of 15 years is the highest. There are corresponding studies concluding that the majority of precipitates are formed in the early stages of thermal aging [12]. Furthermore, these precipitates only coarsen and migrate after formation, so the precipitates are less affects the nanohardness after the early stages of heat treatment.

From the next stage of heat treatment, i.e., heat treatments simulating an operation time of 30 or more years, the characteristics of the grain boundaries and residual strain significantly affect the nanohardness. The increase in low-angle grain boundaries near the type-II boundary could reduce the hardness because precipitates are formed and located at the highly energetic grain boundaries, which are high-angle grain boundaries [12]. Furthermore, the relaxation of residual stress can reduce the hardness.

5. Conclusions

Microstructural, grain boundary orientation, nanohardness analysis were conducted in the type-II boundary and fusion boundary region of the DMW between Alloy 152 and low-alloy steel A533 Gr. B in order to investigate the effect of thermal aging influence.

1) Type-II boundaries are observed in the whole specimen, which seem to be arranged and then shifted away from fusion boundary as the heat treatment is applied.

2) Increasing low-angle grain boundaries were observed as the heat treatment proceeded. The GAM has the highest value at the narrow zone between the type-II boundary and fusion boundary.

3) Chromium contents increased in the weld metal side of the DMW as the heat treatment was applied. At as-welded state, the region showing the chemical gradient such as chromium dilution zone was formed in the span of about 1500-μm from fusion boundary and it had been decreased with heat treatment progressed.

4) Nanohardness was the highest for the heat treatment simulating an operation time of 15 years. From the changes that occurred during the heat treatment, we infer that different parameters affect the nanohardness at each stage of the heat treatment.

5) At the early stage of thermal aging, i.e. until operation time of 15 years, the increase of hardness was observed and the reason for this might be the precipitation of chromium carbide. In contrast, from the next stage of thermal aging, i.e. operation time of 30 years or more years, the decrease of hardness was observed and the reason for this might be the increase of the low angle grain boundaries and release of residual stress. It seems that the effect of the precipitation during heat treatment is lower than that of low angle grain boundary and residual stress.

ACKNOWLEDGMENTS

This work was financially supported by the Nuclear Power Core Technology Development Program (No.20131520000140) and International Collaborative Energy Technology R&D Program (No.20138530030010) of the Korea Institute of Energy Technology Evaluation and Planning (KETEP) granted financial resource from the Ministry of Trade Industry and Energy and by the R&D program organized by the National Research Foundation (NRF) of Korea in support of the Ministry of Science, ICT and Future Planning.

REFERENCES

[1] Li, G.F., Charles, E.A., Congleton, J., 2001, “Effect of post weld heat treatment on stress corrosion cracking of a low alloy steel to stainless steel transition weld.”, Corrosion Science, 43, pp. 1963-1983.

[2] Seifert, H.P., Ritter, S., Shoji, T., Peng, Q.J., Takeda, Y., Lu, Z.P., 2008, "Environmentally-assisted cracking behavior in the transition region of an Alloy182/SA 508 Cl.2 dissimilar metal weld joint in simulated boiling water reactor normal water chemistry environment", Journal of Nuclear Materials, 378, pp. 197-210.

[3] Nelson, T.W., Lippold, J.C., Mills, M.J., 2000, "Nature and evolution of the fusion boundary in ferritic-austenitic dissimilar metal welds – Part 2: On-cooling transformations", Welding Journal, 79, pp. 267-277.

[4] Hou, J., Peng, Q.J., Takeda, Y., Kuniya, J., Shoji, T., Wang, J.Q., Han, E.H., Ke, W., 2010, "Microstructure and mechanical property of the fusion boundary region in an alloy 182-low alloy steel dissimilar weld joint", Journal of Material Science, 45, pp. 5332-5339

[5] Hou, J., Peng, Q.J., Takeda, Y., Kuniya, J., Shoji, T., Wang, J.Q., Han, E.H., Ke, W., 2010, "Microstructure and stress corrosion cracking of the fusion boundary region in an alloy 182-A533B low alloy steel dissimilar weld joint", Corrosion Science, 52, pp. 3949-3954.

[6] 2010, "2010 ASME Boiler and Pressure Vessel Code, Section IX: Welding and Brazing Qualifications, Includes 2011 Addenda Reprint", American Society of Mechanical Engineers.

[7] Choi, K.J., Kim, J.J., Lee, B.H., Bahn, C.B., Kim, J.H., 2013, "Effects of thermal aging on microstructures of low alloy steel-Ni base alloy dissimilar metal weld interfaces", Journal of Nuclear Materials, 441, pp. 493-502.

[8] Boursier, J.M., Vaillant, F., Yrieix, B., 2004, "Weldability, thermal aging and PWSCC behavior of nickel weld metals containing 15 to 30% chromium", American Society of Mechanical Engineers, Pressure Vessels and Piping Division, 490, pp. 109-121.

[9] Peng, Q.J., Shoji, T., Yamauchi, H., Takeda, Y., 2007, "Intergranular environmentally assisted cracking of Alloy 182 weld metal in simulated normal water chemistry of boiling water reactor", Corrosion Science, 49, pp. 2767-2780.

[10] Kamaya, M., 2011, "Assessment of local deformation using EBSD: Quantification of accuracy of measurement and definition of local gradient", Ultramicroscopy, 111, pp. 1189-1199.

[11] Peng.Q.J., Xue, H., Hou, J., Sakaguchi, K., Takeda, Y., Kuniya, Shoji, T., 2011, "Role of water chemistry and microstructure in stress corrosion cracking in the fusion boundary region of an alloy 182-A533B low alloy steel dissimilar weld joint in high temperature water", Corrosion Science, 53, pp. 4309-4317.

[12] Mo, K., Lovicu, G., Tung, H.M., Chen, X., Stubbins, J.F., 2011, "High temperature aging and corrosion study on alloy 617 and alloy 230", Journal of Engineering for Gas Turbines and Power, 133, pp. 052908-1 – 052098-9.